

# Transient convective uplift of an ancient buried landscape

Ross A. Hartley<sup>1\*</sup>, Gareth G. Roberts<sup>1</sup>, Nicky White<sup>1</sup> and Chris Richardson<sup>2</sup>

**Sedimentary basins in the North Atlantic Ocean preserve a record of intermittent uplift during Cenozoic times<sup>1</sup>. These variations in elevation are thought to result from temperature changes within the underlying Icelandic mantle plume<sup>2</sup>. When parts of the European continental shelf were episodically lifted above sea level, new landscapes were carved by erosion, but these landscapes then subsided and were buried beneath marine sediments<sup>3</sup>. Here, we use three-dimensional seismic data to reconstruct one of these ancient landscapes that formed off the northwest coast of Europe during the Palaeocene-Eocene Thermal Maximum. We identify a drainage network within the landscape and, by modelling the profiles of individual rivers within this network, we reconstruct the history of surface uplift. We show that the landscape was lifted above sea level in a series of three discrete steps of 200–400 m each. After about 1 million years of subaerial exposure, this landscape was reburied. We use the magnitude and duration of uplift to constrain the temperature and velocity of a mantle-plume anomaly that drove landscape formation. We conclude that pulses of hot, chemically depleted, mantle material spread out radially beneath the lithospheric plate at velocities of  $\sim 35 \text{ cm yr}^{-1}$ .**

Despite its importance, the detailed spatial and temporal pattern of convective circulation within the Earth's mantle is poorly understood. One exception is the Icelandic plume, whose present-day structure is known from seismic tomographic studies and from geochemical modelling of basaltic rocks<sup>4–6</sup>. This plume underlies a mid-oceanic ridge, which acts as a linear sampler of the plume's temporal history<sup>1,6</sup>. Recent work shows that short-period ( $\sim 1 \text{ Myr}$ ) thermal anomalies generated within the plume conduit spread out radially to distances of  $\sim 1,000 \text{ km}$  from the plume's centre<sup>7</sup>. These anomalies travel beneath adjacent lithospheric plates and are recorded in sedimentary basins fringing the North Atlantic Ocean<sup>2</sup>. Their stratigraphic and geological expression should contain important information about the size, shape and speed of transient anomalies within convecting plumes.

We describe and analyse a buried landscape that was generated by rapid uplift<sup>3</sup>. This landscape was mapped using a volume of three-dimensional seismic reflection data, which covers  $\sim 10,000 \text{ km}^2$  on the northwest continental shelf of Europe. The landscape is buried  $\sim 2 \text{ km}$  beneath the seabed and formed 57–55 Myr ago at a distance of  $\sim 600 \text{ km}$  from the centre of the Icelandic plume (Fig. 1). To map this irregular surface, we handpicked in-lines and cross-lines (that is, orthogonal vertical slices) every 150 m and tracked the surface throughout the seismic volume. The resultant resolution is  $\sim 30 \text{ m}$ . On a typical in-line, the landscape is characterized by a weak, rugose reflection that occurs beneath a

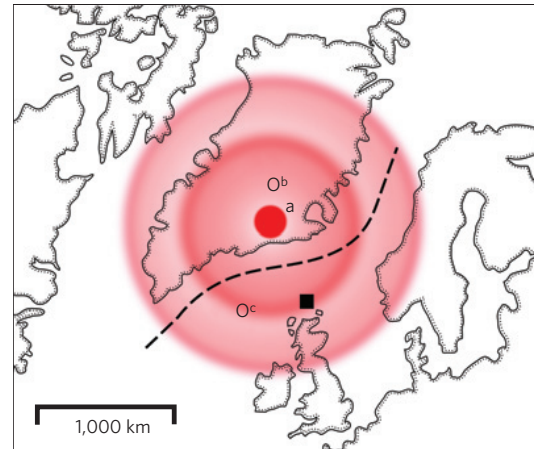


**Figure 1 | Icelandic plume.** Reconstructed palaeogeography of the North Atlantic Ocean during Late Paleocene times<sup>23</sup>. a, b and c are proposed plume centres of ref. 6, ref. 24 and ref. 1, respectively. Dashed black line, location of continental break-up; black square, region of study shown in Fig. 2; red shading, idealized extent of Icelandic plume, where ripples represent radial spreading of hotter annuli of plume material.

package of much stronger reflections (Fig. 2a,b). Later folding of this surface was removed by flattening the volume at the top of the overlying Balder formation. Conversion from two-way travel time to depth was carried out using checkshot surveys from 45 wells that penetrate the seismic volume. The effects of sedimentary compaction were removed using porosity–depth estimates<sup>2</sup>.

The recovered landscape reveals a pattern of dendritic drainage with steep slopes, typical of regions where poorly consolidated sedimentary rocks undergo rapid erosion (Fig. 2c). To the south and east, topographic highs of  $\sim 800 \text{ m}$  above the minimum elevation occur. Drainage divides can be traced along their crests. A broad valley with a meandering channel bisects the landscape and terminates in the foreground at a prominent cliff. Above this valley, a network of branching tributaries is observed. Three prominent surfaces occur at  $\sim 0.5 \text{ km}$ ,  $\sim 0.8 \text{ km}$ ,  $\sim 0.9 \text{ km}$  (that is, green, brown and white shaded surfaces, respectively; Fig. 2c).

This deeply incised landscape is cut into the 58.5–56-Myr-old Lamba formation, which consists of marine deltaic deposits whose flat topset units were deposited at sea level<sup>8</sup>. This formation is largely unreflective and consists of mudstones and siltstones with occasional thin sandy layers. To the south, the landscape progressively oversteps older rocks, notably the  $\sim 58.5\text{-Myr-old}$  Kettle Member, a tuffaceous layer located at the base of the

<sup>1</sup>Bullard Laboratories, Madingley Rise, Madingley Road, Cambridge, CB3 0EZ, UK, <sup>2</sup>BP Institute, Madingley Rise, Madingley Road, Cambridge, CB3 0EZ, UK. \*e-mail: rah68@cam.ac.uk

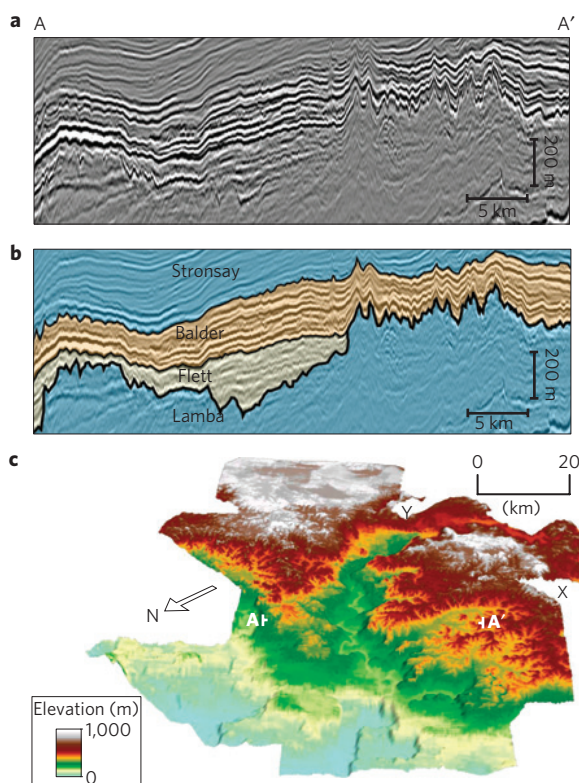


**Figure 2 | Seismic imaging of buried landscape.** **a**, Vertical slice through three-dimensional seismic volume. The water depth is  $\sim 900$  m and the top of the slice is  $\sim 700$  m beneath the seabed. Black and white bands, reflectivity changes caused by lithological variation. **b**, Geological interpretation. Blue and yellow, marine and terrestrial rocks respectively. Thick line, landscape cut into marine Lamba deposits; thin lines, top of terrestrial Flett and Balder formations. **c**, Perspective view of landscape. Note surfaces at  $\sim 0.5$  km (green),  $\sim 0.8$  km (brown) and  $\sim 0.9$  km (white). A–A', vertical slice. X and Y, orientation aids (see Fig. 3).

1 Lamba formation. The eroded landscape has been infilled by the  
 2 56–54.5 Myr Flett and Balder formations. During the early stages,  
 3 pollen assemblages and an absence of marine microfauna indicate  
 4 that terrestrial conditions prevailed. Occasionally, thin mudstones  
 5 containing dinocysts suggest that short-lived marine transgressions  
 6 occurred<sup>9</sup>. To the north, the Flett formation lies conformably on the  
 7 Lamba formation and there is little evidence for drainage incision.  
 8 This limit of conformable contact is interpreted as the ancient  
 9 coastline. It coincides with the prominent topographic step and  
 10 with the basinward extent of Lamba delta lobes<sup>2</sup>. Further south,  
 11 the Flett formation disappears and the landscape is overlain by  
 12 mudstones and sandstones of the Balder formation. These rocks  
 13 contain lignites and oxidized soil horizons, which confirm that the  
 14 incised surface is terrestrial<sup>9</sup>. The Balder formation is overlain  
 15 by marine mudstones of the Stronsay group.

16 These stratigraphic observations show that a buried landscape  
 17 was generated by transient uplift that lasted 2–3 Myr. Surface  
 18 envelope mapping indicates that the minimum amount of uplift  
 19 is 550 m<sup>2</sup>, which rules out glacio-eustatic mechanisms<sup>10</sup>. Instead,  
 20 the landscape could have formed when a thermal anomaly flowed  
 21 beneath the lithospheric plate. The structure of this thermal  
 22 anomaly can be determined by analysing the uplift history of  
 23 the buried landscape. We reconstructed the drainage pattern by  
 24 calculating flow directions across the landscape<sup>11</sup>. This pattern  
 25 shows that eight tributaries and their catchments drain the  
 26 landscape (Fig. 3). Longitudinal profiles (that is, height plotted as  
 27 a function of upstream distance) reveal that each tributary has

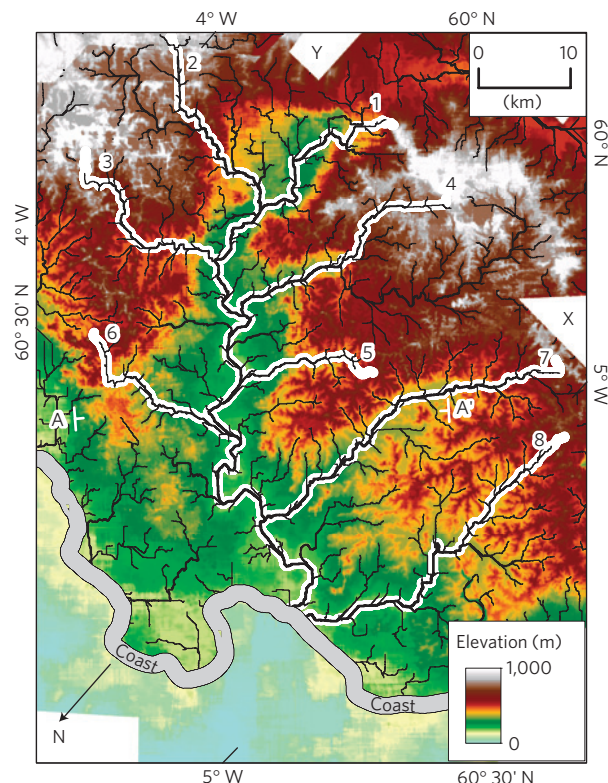


**Figure 3 | Topographic map of buried landscape.** Numbered black-on-white lines, eight river tributaries traced out by a flow-routing algorithm that reconstructs drainage networks from digital elevation models<sup>11</sup>; grey band, inferred coastline<sup>2</sup>. A–A', position of vertical slice shown in Fig. 2a; X and Y, orientation aids (Fig. 2c). The line spacing of seismic data is typically 30 m.

a series of knickzones (that is, rapid gradient changes), which  
 28 match the three prominent surfaces visible in the incised landscape  
 29 (Fig. 4a). Given the similarity of each profile and the homogeneity  
 30 of the underlying Lamba formation, it is unlikely that these  
 31 surfaces and knickzones are lithologically controlled. Instead, the  
 32 youthfulness of these longitudinal profiles indicates that polyphase  
 33 uplift was short lived.  
 34

We have used these longitudinal profiles to calculate an uplift  
 35 history<sup>12,13</sup>. The rate of change of elevation along a river profile,  
 36  $\partial z/\partial t$ , is given by  
 37

$$\frac{\partial z}{\partial t} = U(t) - vA^m \frac{\partial z}{\partial x} + \kappa \frac{\partial^2 z}{\partial x^2} \quad (1) \quad 38$$

where  $U(t)$  is the uplift rate as a function of time only,  $vA^m$  is the  
 39 knickzone velocity,  $A$  is the upstream drainage area at any distance  
 40  $x$ ,  $m$  is an erosional constant,  $v$  is an advective constant and  $\kappa$  is the  
 41 diffusivity (Supplementary Information). In ref. 13 it is shown that  
 42 the most important erosional parameters are  $m$  and  $v$ , which trade  
 43 off negatively against each other. Here, their values are constrained  
 44 by the duration of landscape exposure, which is  $\sim 2.5$  Myr.  $m$  is  
 45 usually assumed to be 0.5 and so  $v = 4.75 \text{ Myr}^{-1}$ . This estimate is  
 46 consistent with rapid erosion rates expected when a landscape is cut  
 47 into relatively unconsolidated sediments<sup>14–16</sup>. Crucially, different  
 48 values of  $m$  and  $v$  do not significantly alter our results, provided that  
 49 the knickzone velocity is consistent with the duration of landscape  
 50 exposure.  $A$  is measured directly from the drainage network.  
 51

The inverse problem is solved by varying  $U(t)$  until the  
 52 misfit between observed and calculated longitudinal profiles is  
 53 minimized (Fig. 4). Longitudinal profiles are accurately matched  
 54 if three discrete phases of uplift are included. These phases have  
 55

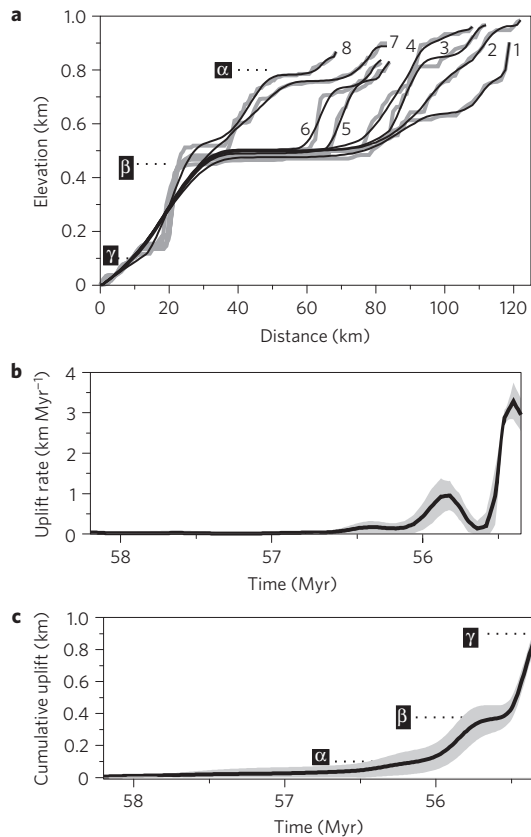


**Figure 4 | Uplift histories.** **a**, River profile modelling. Grey numbered lines, observed profiles (Fig. 3); black lines, calculated profiles obtained by varying uplift rate history. Knickzones along river profiles bound low-relief surfaces labelled  $\alpha$ ,  $\beta$  and  $\gamma$  (Fig. 2c). **b**, Uplift rate history. Black line, uplift rate history calculated from river profiles; grey band,  $1\sigma$  uncertainty reflecting variation of erosional parameters. **c**, Cumulative uplift history (that is  $\int_0^t U dt$ ). Black line, cumulative uplift history; grey band,  $1\sigma$  uncertainty.

1 peak uplift rates of 0.5, 1 and 3  $\text{mm yr}^{-1}$ , which produce the  
 2 three elevated surfaces visible in Fig. 2c. The uncertainty envelope  
 3 for  $U(t)$  was calculated by Monte Carlo inversion, whereby 50  
 4 inversions were carried out for randomly varying values of  $m$ ,  
 5  $\nu$  and  $\kappa$ . Total uplift is consistent with previously published  
 6 estimates<sup>2,17</sup>. Our reconstructed history suggests that uplift peaked  
 7 at  $\sim 55.5$  Myr (Fig. 5). Rapid subsidence ensued and the incised  
 8 landscape was quickly buried.

9 This complex, transient uplift event can be attributed to the  
 10 passage of a hot annulus of plume material beneath the lithospheric  
 11 plate. A similar uplift event is observed 240 km away in the North  
 12 Sea at 54.5 Myr (ref. 18), which prescribes a radial flow velocity of  
 13  $\sim 35 \text{ cm yr}^{-1}$  beneath the region we have mapped. In a kinematic  
 14 model of constant flux<sup>19</sup>, slugs of hot mantle travel up the plume  
 15 conduit and then spread out radially by Poiseuille flow. Regional  
 16 uplift,  $U$ , is given by

$$U = \frac{2h\alpha\bar{T}}{1-\alpha T_0} \quad (2)$$

18 where  $\bar{T}$  is the average temperature anomaly,  $T_0$  is the ambi-  
 19 ent temperature of the plume,  $2h$  is the thickness of the  
 20 convective layer and  $\alpha$  is the thermal expansion coefficient  
 21 (Supplementary Information).

22 Our polyphase uplift history suggests that this convective  
 23 anomaly has a complex internal structure. A simple explanation  
 24 is that it consists of a series of increasingly hot blobs generated

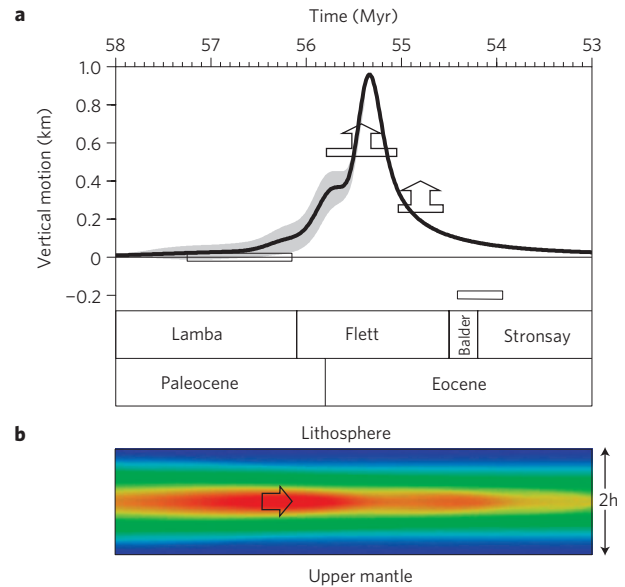


**Figure 5 | Model of transient vertical motion.** **a**, Observed and calculated uplift histories. Grey band, uplift history determined from river profiles (Fig. 4); open rectangles with arrows, stratigraphic constraints<sup>2</sup>; solid black line, best-fitting uplift history calculated from complex pulse of hot material<sup>19</sup>. The region subsides by  $\sim 200$  m between 58 and 53 Myr owing to post-rift subsidence. **b**, Vertical slice through dynamic model of radial flow, where  $2h = 200$  km (ref. 25). Viscosity,  $\nu$ , varies with temperature,  $T$ , where  $\nu(T) = \nu_0 \exp(B\Delta T)$  with  $B = 0.025$ .  $\Delta T$  is the difference between the highest temperature and  $T$ . The input is represented as three Gaussian pulses, characterized by height,  $S$ , and half-width,  $\delta$  (Supplementary Information; ref. 19). The time delay between pulses is  $\sim 0.4$  Myr and their speed is set by the area flux,  $q$  (Supplementary Information).

within the conduit of the plume, which flow radially outwards. 25  
 As the Péclet number is  $\sim 4 \times 10^4$ , radial advection dominates 26  
 and a tripartite thermal structure will not diffuse away over 27  
 distances of 600 km (ref. 19). Instead, internal structure is 28  
 preserved and polyphase uplift is generated. This explanation is 29  
 corroborated by the present-day structure of V-shaped ridges south 30  
 of Iceland, where there is evidence for compound, multistranded 31  
 morphologies that require composite thermal anomalies<sup>7,20</sup>. We use 32  
 an analytical expression to calculate the temperature structure of 33  
 the thermal anomaly required to fit the uplift history<sup>19</sup> (Fig. 5a). In 34  
 this kinematic analysis, the thermal anomaly is made up of three 35  
 closely spaced hot blobs with average excess temperatures of 15, 36  
 60 and  $130^\circ\text{C}$  (see also Supplementary Information). Agreement 37  
 between theory and observation is good. At 600 km from the 38  
 plume centre, the ambient plume temperature is  $\sim 1,330^\circ\text{C}$  so 39  
 the hottest blob has a temperature of  $\sim 1,460^\circ\text{C}$ . This value 40  
 can be reduced if plume material within the thermal anomaly 41  
 is compositionally buoyant. Numerical experiments on plume 42  
 conduits suggest that depleted upper mantle is entrained into 43  
 plume conduits<sup>21</sup>. As depleted mantle is  $0.15 \text{ Mg m}^{-3}$  lighter than 44  
 lower-mantle material, the average temperature of a hot blob can 45  
 be reduced by  $\sim 50^\circ\text{C}$  if up to one-half of the thermal anomaly 46  
 consists of depleted material. Our kinematic analysis is supported by 47  
 a fluid dynamical numerical experiment that assumes that hot blobs 48  
 travel radially outwards in a horizontal layer with depth-dependent 49  
 viscosity (Fig. 5b). This dynamical simulation shows that composite 50  
 thermal anomalies maintain their internal structure up to  $\sim 600$  km 51  
 from the plume conduit. 52

In conclusion, we have mapped and analysed a spectacular 53  
 buried landscape, which contains important clues about otherwise 54  
 inaccessible details of convective circulation within the Earth's 55

1 mantle. Polyphase uplift and subsidence of the landscape show  
2 that a composite thermal anomaly flowed horizontally beneath  
3 the lithospheric plate. Such anomalies are probably generated  
4 by the interaction of discrete solitary waves that flow up plume  
5 conduits<sup>22</sup>. Although the existence of solitary waves has been  
6 predicted, their passage beneath fringing continental margins as  
7 well as our ability to observe their stratigraphic manifestation is  
8 both unexpected and significant.

9 Received 22 February 2010; accepted 27 May 2011;  
10 published online XX Month XXXX

## 11 References

- 12 1. Jones, S. M. & White, N. Shape and size of the starting Iceland plume swell.  
13 *Earth Planet. Sci. Lett.* **216**, 271–282 (2003).
- 14 2. Shaw Champion, M. E., White, N. J., Jones, S. M. & Lovell, J. P. B. Quantifying  
15 transient mantle convective uplift: An example from the Faroe–Shetland basin.  
16 *Tectonics* **27**, TC1002 (2008).
- 17 3. Smallwood, J. R. & Gill, C. E. The rise and fall of the Faroe–Shetland Basin:  
18 Evidence from seismic mapping of the Balder Formation. *J. Geol. Soc. Lond.*  
19 **159**, 627–630 (2002).
- 20 4. Bijwaard, H. & Spakman, W. Tomographic evidence for a narrow whole mantle  
21 plume below Iceland. *Earth Planet. Sci. Lett.* **166**, 121–126 (1999).
- 22 5. Ritsema, J., Deuss, A., van Heijst, H. J. & Woodhouse, J. H. S40RTS: A  
23 degree-40 shear-velocity model for the mantle from new Rayleigh wave  
24 dispersion, teleseismic traveltimes and normal-mode splitting function  
25 measurements. *Geophys. J. Int.* **184**, 1223–1236 (2010).
- 26 6. White, R. & McKenzie, D. Magmatism at rift zones: The generation of volcanic  
27 continental margins and flood basalts. *J. Geophys. Res.* **94**, 7685–7729 (1989).
- 28 7. Poore, H. R., White, N. & Jones, S. A Neogene chronology of Iceland plume  
29 activity from V-shaped ridges. *Earth Planet. Sci. Lett.* **283**, 1–13 (2009).
- 30 8. Mudge, D. C. & Jones, S. M. Palaeocene uplift and subsidence events in the  
31 Scotland–Shetland and North Sea region and their relationship to the Iceland  
32 Plume. *J. Geol. Soc. Lond.* **161**, 381–386 (2004).
- 33 9. Mudge, D. C. & Bujak, J. P. Biostratigraphic evidence for evolving  
34 palaeoenvironments in the Lower Paleogene of the Faroe–Shetland Basin.  
35 *Mar. Petrol. Geol.* **18**, 577–590 (2001).
- 36 10. Miller, K. G. *et al.* The Phanerozoic record of global sea-level change. *Science*  
37 **310**, 1293–1298 (2005).
- 38 11. Tarboton, D. G., Bras, R. L. & Rodriguez-Iturbe, I. On the extraction of channel  
39 networks from digital elevation data. *Hydrol. Process.* **5**, 81–100 (1991).
- 40 12. Pritchard, D., Roberts, G. G., White, N. J. & Richardson, C. N. Uplift histories  
41 from river profiles. *Geophys. Res. Lett.* **36**, L24301 (2009).
- 42 13. Roberts, G. G. & White, N. Estimating uplift rate histories from river profiles  
43 using African examples. *J. Geophys. Res.* **115**, B02406 (2010).

- 44 14. Howard, A. D. & Kerby, G. Channel changes in badlands. *Geol. Soc. Am. Bull.*  
45 **94**, 739–752 (1983).
- 46 15. Yair, A., Goldberg, P. & Brimer, B. Long term denudation rates in the  
47 Zin-Havrim badlands, northern Negev, Israel. *Badland Geomorphol. Piping*  
48 279–291 (1982).
- 49 16. Dadson, S. J. *et al.* Links between erosion, runoff variability and seismicity in  
50 the Taiwan orogen. *Nature* **426**, 648–651 (2003).
- 51 17. Nadin, P. A., Kusnir, N. J. & Cheadle, M. J. Early Tertiary plume uplift  
52 of the North Sea and Faeroe–Shetland Basins. *Earth Planet. Sci. Lett.* **148**,  
53 109–127 (1997).
- 54 18. Underhill, J. R. Controls on the genesis and prospectivity of Paleogene  
55 palaeogeomorphic traps, East Shetland Platform, UK North Sea. *Mar. Petrol.*  
56 *Geol.* **18**, 259–281 (2001).
- 57 19. Rudge, J. F., Shaw Champion, M. E., White, N., McKenzie, D. & Lovell, B.  
58 A plume model of transient diachronous uplift at the Earth's surface. *Earth*  
59 *Planet. Sci. Lett.* **267**, 146–160 (2008).
- 60 20. Ito, G. Reykjanes 'V'-shaped ridges originating from a pulsing and dehydrating  
61 mantle plume. *Nature* **411**, 81–84 (2001).
- 62 21. Hauri, E. H., Whitehead, J. A. & Hart, S. R. Fluid dynamic and  
63 geochemical aspects of entrainment in mantle plumes. *J. Geophys. Res.*  
64 **99**, 24275–24300 (1994).
- 65 22. Schubert, G., Olson, P., Anderson, C. & Goldman, P. Solitary waves in mantle  
66 plumes. *J. Geophys. Res.* **94**, 9523–9532 (1989).
- 67 23. Srivastava, S. P. & Tapscott, C. R. Plate kinematics of the North Atlantic.  
68 *Geol. North Am.* 379–404 (1986).
- 69 24. Lawver, L. A. & Müller, R. D. Iceland hotspot track. *Geology* **22**, 311–314 (1994).
- 70 25. Delorey, A. A., Dunn, R. A. & Gaherty, J. B. Surface wave tomography of the  
71 upper mantle beneath the Reykjanes Ridge with implications for ridge–hot  
72 spot interaction. *J. Geophys. Res.* **112**, B08313 (2007).

## Acknowledgements

This research is funded by the BP–Cambridge margins project. We are grateful to R. Corfield, I. Frame, B. Lovell, D. Lyness, L. Mackay and J. Rudge for their help. M. Gurnis and R. Westaway provided reviews. Figures were prepared using the GMT, InkScape and ArcGIS software packages. Department of Earth Sciences Contribution Number esc.2064.

## Author contributions

All authors contributed equally.

## Additional information

The authors declare no competing financial interests. Supplementary information accompanies this paper on [www.nature.com/naturegeoscience](http://www.nature.com/naturegeoscience). Reprints and permissions information is available online at <http://www.nature.com/reprints>. Correspondence and requests for materials should be addressed to R.A.H.

## Page 1

---

*Query 1: Line no. 1*

Please note that the first paragraph has been edited according to style.

*Query 2: Line no. 8*

As per journal style, reference citations should be in numerical order. Therefore references are renumbered from here onwards. OK?

## Page 3

---

*Query 3: Line no. 21*

Please avoid hyphen at end of first line of column.

*Query 4: Line no. 24*

'size' changed to 'height' in fig. 5 caption—is this correct?